

Robust and efficient primal-dual Newton-Krylov solvers for viscous-plastic sea-ice models

Yu-hsuan Shih^a, Carolin Mehlmann^b, Martin Losch^c, Georg Stadler^a

^a*Courant Institute of Mathematical Sciences, New York University, New York, NY, USA*

^b*Otto-von-Guericke Universität, Magdeburg, Germany*

^c*Alfred-Wegener-Institut, Helmholtz-Zentrum für Polar- und Meeresforschung, Bremerhaven, Germany*

Abstract

We present a Newton-Krylov solver for a viscous-plastic sea-ice model. This constitutive relation is commonly used in climate models to describe the material properties of sea ice. Due to the strong nonlinearity introduced by the material law in the momentum equation, the development of fast, robust and scalable solvers is still a substantial challenge. In this paper, we propose a novel primal-dual Newton linearization for the implicitly-in-time discretized momentum equation. Compared to existing methods, it converges faster and more robustly with respect to mesh refinement, and thus enables numerically converged sea-ice simulations at high resolutions. Combined with an algebraic multigrid-preconditioned Krylov method for the linearized systems, which contain strongly varying coefficients, the resulting solver scales well and can be used in parallel. We present experiments for two challenging test problems and study solver performance for problems with up to 8.4 million spatial unknowns.

Keywords: viscous-plastic rheology, primal-dual, stress-velocity Newton, AMG-preconditioned Krylov, sea-ice, localization

1. Introduction

Satellite images show that the sea-ice cover is characterized by local linear formations, so-called linear kinematic features (LKFs) [27]. These LKFs are associated to leads and pressure ridges (i.e., regions of low or high sea-ice density due to diverging or converging ice motion) and play a major role on sea-ice formation and the ocean-ice-atmosphere interaction. To represent LKFs in sea-ice models, the sea-ice rheology plays a crucial role. Most sea-ice models used in climate studies treat sea-ice as a continuum with a viscous-plastic (VP) constitutive law [7], although alternative rheologies have been suggested [15, 38, 45]. These approaches are all based on the continuum assumption, which implies that statistical averages can be derived from a large number of ice floes. The underlying assumptions of the continuum approach break down at high resolutions and there are recently suggested approaches that resolve discrete floes [12, 17, 46–48]. However, the majority of sea-ice models in climate simulations are still using the VP rheology and will do so in the foreseeable future [7]. Recent analyses demonstrated that models based on the VP rheology reproduce scaling and statistics of observed LKFs [21]. However, resolving LKFs in the viscous-plastic sea-ice model is computationally very costly as LKFs require high spatial resolution [25, 28]. Furthermore, the VP sea-ice model is stiff and resolving LKFs typically requires that a non-linear solver performs a large number of iterations, and this number grows with increasing mesh resolution.

Viscous-plastic sea-ice solvers. Currently there are mainly two solution approaches for VP sea-ice models. Firstly, and most commonly, explicit time stepping procedures for the momentum equation are used. Here, as proposed by [20], pseudo-elastic terms are added to sea-ice stresses, which leads to the elastic-viscous-plastic (EVP) method. The additional pseudo-elastic term increases the order of the time derivative of the coupled momentum-stress equations, making the system less stiff and thus numerically easier to solve. The resulting momentum equation can be integrated explicitly, albeit using a large number of small time steps for each outer time step of the sea-ice model.

With recent modifications to EVP [8, 23, 28], accurate VP solutions are possible in principle, but because the convergence rate of the method is linear and slow for high resolution simulations, practical solvers limit the number of iterations and hence the accuracy [25]. In spite of this, EVP is the most commonly used method of solving the momentum equation in sea-ice climate models. Secondly, implicit methods for the momentum equation are used. These range from the application of a few Picard iterations per time step [51], to more sophisticated Newton solvers with better convergence properties [30, 32, 36]. Fully converged solutions with Newton solvers are still very expensive for climate-type applications, which is why they have been mostly used as reference solutions for the VP model to evaluate non-optimal solvers such as EVP [e.g., 24, 28].

Typically, the simulation time per unknown increases substantially with the problem size for both, available explicit and implicit solvers. For explicit solvers, this is due to the fact that resolving the VP rheology requires an increasing number of small time steps, and solver stabilization depends on the spatial discretization and hence results in a slower convergence [13, 23]. For implicit solvers, typically the number of Newton or Picard iterations increases upon mesh refinement, and the linearized systems become more ill-conditioned and thus iterative linear solvers converge more slowly. Direct linear solvers do not suffer from this limitation, but they cannot be used for large systems due to memory limitations. Even when memory is not a limiting factor, the solve time of direct linear solvers grows substantially faster-than-linear with the number of unknowns. Currently used solvers for the linearized system include relaxation methods such as the line successive over-relaxation [29, 32, 51] and geometric multigrid [35].

Approach and related work. In this paper, we focus on implicit Newton-type solvers for the momentum equation. We address the common growth of nonlinear and linear iterations for increasing problems size through (1) a novel Newton linearization, and (2) the use of algebraic multigrid (AMG) preconditioning for the arising linear problems. The novel Newton iteration is based on a temporary introduction of an independent stress variable during the linearization. This idea is similar to the introduction of a dual variable in primal-dual interior point methods [49]. For nonlinear physics problems, similar approaches have successfully been used for non-Newtonian fluids [40, 43] or total variation image regularization [10, 19]. To solve the large-scale linear matrix systems arising upon linearization, we propose an AMG-preconditioned Krylov solver. Since these systems involve strongly varying and anisotropic coefficients as results of the VP constitutive relation, we find it beneficial to adjust default parameters in AMG, for which we use the parallel HyPre library [14].

Contributions and limitations. In this paper, we make the following contributions. (1) We propose an alternative Newton linearization for the sea-ice momentum equation whose number of Newton steps is insensitive to the mesh resolution and to regularization parameters. (2) We propose an AMG-preconditioned Krylov method to solve the Newton linearizations efficiently and in parallel and present results for problems with up to 8.4 million spatial unknowns. (3) We provide an implementation of our method in the open-source Firedrake library and present performance comparisons with other commonly used sea-ice solvers for benchmark problems.

Our approach also has some limitations. (1) The proposed method requires the introduction of an additional tensor variable. However, this variable is updated explicitly and the linear systems to be solved in each Newton step are of the same size as for other Newton or Picard methods. (2) Despite substantial improvements, we do not achieve perfect weak scalability, i.e., when the unknowns and the compute resources are increased at the same rate, the solution time does not remain constant but increases, although moderately. Besides known challenges to achieving perfect scalability, this is also due to the fact that upon mesh refinement, the VP constitutive relation yields ever-smaller features, making the physics problem more challenging.

2. Governing Equations

Let $\Omega \subset \mathbb{R}^2$ be the spatial sea-ice domain, and $I_t := [0, T] \subset \mathbb{R}$ the time interval over which we consider the sea-ice evolution. Following [18], we consider the following system of equations for the sea-ice concentration $A(t, \mathbf{x}) \in [0, 1]$, the mean sea-ice thickness $H(t, \mathbf{x}) \geq 0$ and sea-ice velocity $\mathbf{v}(t, \mathbf{x}) \in \mathbb{R}^2$,

for all $(t, \mathbf{x}) \in I_t \times \Omega$:

$$\rho_{\text{ice}} H (\partial_t \mathbf{v} + f_c \mathbf{e}_r \times (\mathbf{v} - \mathbf{v}_o)) = \nabla \cdot \boldsymbol{\sigma} + \boldsymbol{\tau}_{\text{ocean}}(\mathbf{v}, t) + \boldsymbol{\tau}_{\text{atm}}(t) \quad \text{in } (0, T) \times \Omega, \quad (1a)$$

$$\partial_t A + \nabla \cdot (\mathbf{v} A) = 0 \quad \text{in } (0, T) \times \Omega, \quad (1b)$$

$$\partial_t H + \nabla \cdot (\mathbf{v} H) = 0 \quad \text{in } (0, T) \times \Omega, \quad (1c)$$

where ρ_{ice} are a given sea-ice density, f_c is the Coriolis parameter and \mathbf{e}_r is the unit vector normal to the surface. The internal stresses $\boldsymbol{\sigma} = \boldsymbol{\sigma}(\mathbf{v}, A, H)$ in the sea-ice are modeled by the VP rheology, [18]

$$\boldsymbol{\sigma} := 2\eta \dot{\boldsymbol{\epsilon}}'(\mathbf{v}) + \zeta \text{tr}(\dot{\boldsymbol{\epsilon}}(\mathbf{v})) \mathbf{I} - \frac{P}{2} \mathbf{I} \quad (2)$$

with viscosities η, ζ given by

$$\eta = e^{-2} \zeta, \quad \zeta = \frac{P}{2\Delta(\mathbf{v})}, \quad \text{where}$$

$$\Delta(\mathbf{v}) := \sqrt{2e^{-2} \dot{\boldsymbol{\epsilon}}'(\mathbf{v}) : \dot{\boldsymbol{\epsilon}}'(\mathbf{v}) + \text{tr}(\dot{\boldsymbol{\epsilon}}(\mathbf{v}))^2 + \Delta_{\min}^2}, \quad (3)$$

$\dot{\boldsymbol{\epsilon}}(\mathbf{v}) := \frac{1}{2}(\nabla \mathbf{v} + \nabla \mathbf{v}^T) \in \mathbb{R}^{2 \times 2}$ is the strain rate tensor, $\dot{\boldsymbol{\epsilon}}'(\mathbf{v}) := \dot{\boldsymbol{\epsilon}}(\mathbf{v}) - \frac{1}{2} \text{tr}(\dot{\boldsymbol{\epsilon}}(\mathbf{v})) \mathbf{I} \in \mathbb{R}^{2 \times 2}$ is the deviatoric strain rate tensor and “:” denotes the Frobenius inner product between tensors. Moreover, $e > 0$ is the ratio of the main axes of the elliptic yield curve (typically, $e = 2$). Following [26], we use a smooth transition between plastic and viscous states using a small constant $\Delta_{\min} > 0$ in (3). The spatially varying ice strength $P = P(\mathbf{x})$ is modeled as

$$P = P^* H \exp(-C(1 - A)) \quad (4)$$

with constants P^* and C . The forcing from atmosphere and ocean are given by

$$\boldsymbol{\tau}_{\text{atm}}(t) = C_a \rho_a \|\mathbf{v}_a(t)\|_2 \mathbf{v}_a(t) \quad \text{and} \quad \boldsymbol{\tau}_{\text{ocean}}(\mathbf{v}, t) = C_o \rho_o \|\mathbf{v}_o(t) - \mathbf{v}\|_2 (\mathbf{v}_o(t) - \mathbf{v}), \quad (5)$$

respectively, where $\|\cdot\|_2$ denotes the Euclidean norm, C_a and C_o are the atmospheric and ocean drag coefficients, ρ_a and ρ_o the densities, and \mathbf{v}_a and \mathbf{v}_o the velocity fields of near surface atmospheric and oceanic flows.

To complete the formulation of the sea-ice system, we use the following initial and boundary conditions:

$$\begin{aligned} \mathbf{v} &= \mathbf{v}_0 && \text{on } \{t = 0\} \times \Omega, \\ A &= A_0, \quad H = H_0 && \text{on } \{t = 0\} \times \Omega, \\ \mathbf{v} &= \mathbf{0} && \text{on } I_t \times \partial\Omega, \\ A &= A^{\text{in}}, \quad H = H^{\text{in}} && \text{on } I_t \times \Gamma^{\text{in}}, \end{aligned}$$

where $\Gamma_{\text{in}} := \{\mathbf{x} \in \partial\Omega \mid \mathbf{n} \cdot \mathbf{v} < 0\}$ denotes the part of the boundary $\partial\Omega$ with incoming characteristics. Recently, analytical results these equations have been reported [9, 31]. However, we focus on the classical system equations (1) and study solvers for the time-discretized equations.

3. Time discretization and implicit momentum equation time step

To discretize (1) in time, we use an explicit method for the hyperbolic equations (1b) and (1c), and an implicit method for the momentum equation (1a). That is, given the triple (\mathbf{v}^n, A^n, H^n) at time t_n , these variables are advanced to time $t_{n+1} := t_n + \delta t$ as follows. First, an explicit time step (e.g., an explicit Euler step) is performed to compute the concentration and height variables A^{n+1} and H^{n+1} , respectively. Due to the stiffness of the momentum equation (1a), using an explicit method for computing the velocity \mathbf{v}^{n+1} requires extremely small time steps [22]. Thus, here we use an implicit time stepping method, namely

the implicit Euler method.¹ Other implicit time stepping methods lead to similar nonlinear problems to be solved in each time step.

Next, we show that the result \mathbf{v}^{n+1} of this implicit step can also be found as minimizer of an appropriately chosen convex energy minimization problem. The formulation as an energy minimization problem builds on [33, 36, 41], where it is shown that the stress tensor can be represented in symmetric form and the derivative of the momentum equation is positive definite, indicating the underlying energy minimization problem. We consider the functional $\Phi : V \rightarrow \mathbb{R}$ defined over a function space $V \supset H_0^1(\Omega)^2$.

$$\begin{aligned} \Phi(\mathbf{v}) := & \int_{\Omega} \frac{1}{2} \rho_{\text{ice}} H^{n+1} \|\mathbf{v}\|_2^2 d\mathbf{x} - \int_{\Omega} \rho_{\text{ice}} H^{n+1} \mathbf{v}^n \cdot \mathbf{v} d\mathbf{x} \\ & + \delta t \left(\int_{\Omega} \frac{P^{n+1}}{2} [\Delta(\mathbf{v}) - \text{tr}(\dot{\epsilon}(\mathbf{v}))] d\mathbf{x} + \int_{\Omega} \frac{1}{3} C_o \rho_o \|\mathbf{v}_o - \mathbf{v}\|_2^3 d\mathbf{x} \right) \\ & + \delta t \left(\int_{\Omega} \rho_{\text{ice}} H^{n+1} f_c \mathbf{e}_r \times (\mathbf{v}^n - \mathbf{v}_o) \cdot \mathbf{v} d\mathbf{x} - \int_{\Omega} \boldsymbol{\tau}_{\text{atm}}(t_{n+1}) \cdot \mathbf{v} d\mathbf{x} \right). \end{aligned} \quad (6)$$

Note that the space V over which Φ is well-defined is slightly larger than $H_0^1(\Omega)^2$ as a finite value of $\Phi(\mathbf{v})$ does not require that \mathbf{v} has square-integrable derivatives. Identifying the appropriate space V for the semi-discretized problem rigorously and proving solution existence/uniqueness is beyond the scope of this paper. We refer to comments in [33] and for a function space analysis of the time-continuous problem to [9, 31]. However, in the next theorem we show that Φ is convex and bounded from below, and that the implicit time step equations can be derived as first-order necessary conditions for a minimizer of Φ . For simplicity, we restrict ourselves to $\mathbf{v} \in H_0^1(\Omega)^2$.

Theorem 1. The functional Φ defined in (6) is convex and bounded from below. Moreover, the solution at next time step $\mathbf{v}^{n+1} \in V$ satisfies the stationary condition $\Phi'(\mathbf{v}^{n+1})(\boldsymbol{\phi}) = 0$ for all $\boldsymbol{\phi} \in V$.

Proof. The functional Φ is convex in the velocity \mathbf{v} and in the strainrate tensor $\dot{\epsilon}(\mathbf{v})$. This follows since the terms in (6) are either linear in \mathbf{v} , or quadratic or cubic in $\|\mathbf{v}\|$, and since $\Delta(\mathbf{v})$ is convex in $\dot{\epsilon}(\mathbf{v})$, which itself is a convex function of \mathbf{v} . Moreover, the coefficients of the quadratic and cubic terms are pointwise non-negative. The functional is bounded from below as terms in which \mathbf{v} appears linearly are dominated by quadratic or third-order terms in \mathbf{v} . Moreover, $\Delta(\mathbf{v}) - \text{tr}(\dot{\epsilon}(\mathbf{v})) \geq 0$ for all $\mathbf{x} \in \Omega$ by definition of $\Delta(\mathbf{v})$.

Let us now compute the first variations of $\Phi(\mathbf{v})$, i.e., $\Phi'(\mathbf{v})(\boldsymbol{\phi})$ following basic methods from variational calculus. For this purpose, we use the identities

$$\begin{aligned} \left(\frac{1}{2} \rho_{\text{ice}} H^{n+1} \|\mathbf{v}\|_2^2 \right)'(\mathbf{v})(\boldsymbol{\phi}) &= \rho_{\text{ice}} H^{n+1} \mathbf{v} \cdot \boldsymbol{\phi}, \\ \left(\frac{1}{3} C_o \rho_o \|\mathbf{v}_o - \mathbf{v}\|_2^3 \right)'(\mathbf{v})(\boldsymbol{\phi}) &= C_o \rho_o \|\mathbf{v}_o - \mathbf{v}\|_2^2 (\|\mathbf{v}_o - \mathbf{v}\|_2)'(\mathbf{v})(\boldsymbol{\phi}) = C_o \rho_o \|\mathbf{v}_o - \mathbf{v}\|_2 (\mathbf{v}_o - \mathbf{v}) \cdot \boldsymbol{\phi}, \\ \left(\frac{P^{n+1}}{2} \Delta(\mathbf{v}) \right)'(\mathbf{v})(\boldsymbol{\phi}) &= \frac{P^{n+1}}{4\Delta(\mathbf{v})} \left(2e^{-2} \dot{\epsilon}'(\mathbf{v}) : \dot{\epsilon}'(\mathbf{v}) + \text{tr}(\dot{\epsilon}(\mathbf{v}))^2 + \Delta_{\min}^2 \right)'(\mathbf{v})(\boldsymbol{\phi}) \\ &= \frac{P^{n+1}}{4\Delta(\mathbf{v})} 4e^{-2} \dot{\epsilon}'(\mathbf{v}) : \dot{\epsilon}'(\boldsymbol{\phi}) + \frac{P^{n+1}}{2\Delta(\mathbf{v})} \text{tr}(\dot{\epsilon}(\mathbf{v})) \text{tr}(\dot{\epsilon}(\boldsymbol{\phi})) \\ &= 2\eta \dot{\epsilon}'(\mathbf{v}) : \dot{\epsilon}'(\boldsymbol{\phi}) + \zeta \text{tr}(\dot{\epsilon}(\mathbf{v})) \text{tr}(\dot{\epsilon}(\boldsymbol{\phi})) \\ &= (2\eta \dot{\epsilon}'(\mathbf{v}) + \zeta \text{tr}(\dot{\epsilon}(\mathbf{v})) \mathbf{I}) : \nabla \boldsymbol{\phi}. \end{aligned} \quad (7)$$

Note that above we used that $\dot{\epsilon}' : \mathbf{I} = 0$. Thus, $\Phi'(\mathbf{v})(\boldsymbol{\phi}) = 0$ is equivalent to

$$\mathcal{A}(\mathbf{v}^{n+1}, \boldsymbol{\phi}) = F(\boldsymbol{\phi}), \quad (8a)$$

¹As not uncommon in sea ice models, the (typically small) Coriolis force term is treated explicitly. This results in a symmetric system matrix.

where $\mathcal{A}(\cdot, \cdot)$ and $F(\cdot)$ are defined as

$$\mathcal{A}(\mathbf{v}^{n+1}, \phi) := (\rho_{\text{ice}} H^{n+1} \mathbf{v}^{n+1}, \phi) + \delta t (\boldsymbol{\sigma}(\mathbf{v}^{n+1}, A^{n+1}, H^{n+1}), \nabla \phi) - \delta t (\boldsymbol{\tau}_{\text{ocean}}(\mathbf{v}^{n+1})), \quad (8b)$$

$$F(\phi) := (\rho_{\text{ice}} H^{n+1} \mathbf{v}^n, \phi) - \delta t (\rho_{\text{ice}} H^{n+1} f_c \mathbf{e}_r \times (\mathbf{v}^n - \mathbf{v}_o), \phi) + \delta t (\boldsymbol{\tau}_{\text{atm}}(t_{n+1}), \phi). \quad (8c)$$

Here, (\cdot, \cdot) denotes the standard L_2 -inner product for vectors or matrices. Thus, (8a)–(8c) is also the weak form of an implicit time step for the momentum equation (1a). \square

The above results shows that the new time level \mathbf{v}^{n+1} can be found by solving

$$\min_{\mathbf{v} \in V} \Phi(\mathbf{v}) \quad (9)$$

with an appropriately defined function space V . Such a variational calculus perspective may be useful to establish rigorous existence and uniqueness results for (8a). If V is approximated by a finite-dimensional space V_h , e.g., a space of piecewise polynomials as common in finite element methods, then it is straightforward to show that the (now fully discrete) time step \mathbf{v}_h^{n+1} is the solution to a finite-dimensional convex optimization problem.

The optimization formulation (9) also shows that the linearization of (8a), which is the second variation of Φ , must be symmetric. This is also discussed in [36]. Additionally, the objective $\Phi(\cdot)$ can also be used in an iterative method to verify that progress has been made towards the computation of \mathbf{v}^{n+1} . In particular, we use decay with respect to Φ in a line search procedure in our Newton methods instead of the more commonly used nonlinear residual norm.

Note that solving the momentum equation (8) (or its spatial discretizations) remains challenging due to the nonlinearity reflecting the VP constitutive relation. The main focus of this paper is on Newton-type methods to solve this equation robustly and efficiently. In particular, we will propose a novel linearization method for (8a) in the next section.

4. Newton methods for the momentum equation

For convenience of the notation, we introduce some notation following [33, Eq.(5.13)]. Namely, we define the tensor

$$\boldsymbol{\tau}(\mathbf{v}) := e^{-1} \dot{\boldsymbol{\varepsilon}}' + \frac{1}{2} \text{tr}(\dot{\boldsymbol{\varepsilon}}) \mathbf{I},$$

which allows us to write, since $\dot{\boldsymbol{\varepsilon}}' : \mathbf{I} = 0$, that

$$\Delta(\mathbf{v}) = \sqrt{\Delta_{\min}^2 + 2\boldsymbol{\tau}(\mathbf{v}) : \boldsymbol{\tau}(\mathbf{v})}.$$

Following [33], the term involving $\boldsymbol{\sigma} = \boldsymbol{\sigma}(\mathbf{v}^{n+1}, A^{n+1}, H^{n+1})$ in (8b) can be written as

$$(\boldsymbol{\sigma}, \nabla \phi) = \left(\frac{P^{n+1}}{\Delta(\mathbf{v})} \boldsymbol{\tau}(\mathbf{v}), \boldsymbol{\tau}(\phi) \right) - \left(\frac{P^{n+1}}{2}, \text{tr}(\dot{\boldsymbol{\varepsilon}}(\phi)) \right), \quad (10)$$

where P^{n+1} is the ice strength (4) evaluated at H^{n+1} and A^{n+1} and (\cdot, \cdot) is the L^2 -inner product of two matrix functions.

4.1. Standard Newton method

A Newton step to solve (8a) is of the following form: Compute the Newton update $\tilde{\mathbf{v}} \in V$ such that

$$\mathcal{A}'(\mathbf{v}_l)(\tilde{\mathbf{v}}, \phi) = F(\phi) - A(\mathbf{v}_l, \phi) \quad \text{for all } \phi \in V, \quad (11)$$

and then perform the Newton update step $\mathbf{v}_{l+1} := \mathbf{v}_l + \alpha \tilde{\mathbf{v}}$ with a step length $\alpha \leq 1$. Here, l denotes the index for the Newton iteration to compute the velocity \mathbf{v}^{n+1} . The Jacobian on the left hand side in (11) is given by

$$\begin{aligned} \mathcal{A}'(\mathbf{v}_l)(\tilde{\mathbf{v}}, \phi) &= (\rho_{\text{ice}} H^{n+1} \tilde{\mathbf{v}}, \phi) \\ &+ \delta t \left(\frac{P^{n+1}}{\Delta(\mathbf{v}_l)} \boldsymbol{\tau}(\tilde{\mathbf{v}}), \boldsymbol{\tau}(\phi) \right) - \delta t \left(2P^{n+1} \frac{\boldsymbol{\tau}(\mathbf{v}_l) \otimes \boldsymbol{\tau}(\mathbf{v}_l)}{\Delta(\mathbf{v}_l)^3} \boldsymbol{\tau}(\tilde{\mathbf{v}}), \boldsymbol{\tau}(\phi) \right) - \delta t \boldsymbol{\tau}'_{\text{ocean}}(\mathbf{v}_l)(\tilde{\mathbf{v}}, \phi), \end{aligned} \quad (12a)$$

where

$$\tau'_{\text{ocean}}(\mathbf{v})(\tilde{\mathbf{v}}, \phi) = (-\rho_o C_o \|\mathbf{v}_o - \mathbf{v}\|_2 \tilde{\mathbf{v}}, \phi) + \left(-\rho_o C_o \frac{(\mathbf{v}_o - \mathbf{v})^T \tilde{\mathbf{v}}}{\|\mathbf{v}_o - \mathbf{v}\|_2} (\mathbf{v}_o - \mathbf{v}), \phi \right). \quad (12b)$$

Here, \otimes in (12a) denotes the outer product between two matrices, whose result is a 4th-order tensor, and we have used the identity $(\mathbf{a} : \mathbf{b})\mathbf{c} = (\mathbf{a} \otimes \mathbf{c})\mathbf{b}$ for matrices $\mathbf{a}, \mathbf{b}, \mathbf{c}$. Hence, the term involving \otimes in (12a) equals $\delta t (2P^{n+1}(\Delta(\mathbf{v}_l))^{-3}(\tau(\mathbf{v}_l) : \tau(\tilde{\mathbf{v}}))\tau(\mathbf{v}_l), \tau(\phi)) = \delta t (2P^{n+1}(\Delta(\mathbf{v}_l))^{-3}(\tau(\mathbf{v}_l) : \tau(\tilde{\mathbf{v}})), \tau(\mathbf{v}_l) : \tau(\phi))$, which is also how it is implemented based on weak forms. To summarize, each Newton iteration amounts to solving a linear system with the operator as defined in (12a).

4.2. A stress-velocity Newton method

Next, we present an alternative formulation for the nonlinear equation (8a). The main difference of this formulation is that it uses a reformulation of the VP nonlinearity that is better suited for Newton linearization. To arrive at this alternative formulation, we introduce the independent variable

$$\boldsymbol{\pi} := \frac{\boldsymbol{\tau}(\mathbf{v})}{\sqrt{\Delta_{\min}^2 + 2\boldsymbol{\tau}(\mathbf{v}) : \boldsymbol{\tau}(\mathbf{v})}} \in \mathbb{R}^{2 \times 2}. \quad (13)$$

Since the denominator is always positive, the definition is equivalent to the nonlinear equation

$$\mathbf{r}(\boldsymbol{\pi}, \mathbf{v}) := \boldsymbol{\pi} \sqrt{\Delta_{\min}^2 + 2\boldsymbol{\tau}(\mathbf{v}) : \boldsymbol{\tau}(\mathbf{v})} - \boldsymbol{\tau}(\mathbf{v}) = 0. \quad (14)$$

With this auxiliary variable $\boldsymbol{\pi}$, (10) simplifies to

$$(P^{n+1}\boldsymbol{\pi}, \tau(\phi)) - \left(\frac{P^{n+1}}{2}, \text{tr}(\dot{\epsilon}(\phi)) \right) := B(\mathbf{v}, \boldsymbol{\pi}, \phi). \quad (15)$$

Substituting (15) for (10) in (8a) and adding (16b) as a new equation, we obtain a new formulation of the momentum equation (8a) for unknowns $(\mathbf{v}, \boldsymbol{\pi})$

$$(\rho_{\text{ice}} H^{n+1} \mathbf{v}, \phi) + \delta t B(\mathbf{v}, \boldsymbol{\pi}, \phi) - \delta t (\tau_{\text{ocean}}(\mathbf{v})) = F(\phi) \quad (16a)$$

$$\mathbf{r}(\boldsymbol{\pi}, \mathbf{v}) = 0. \quad (16b)$$

The corresponding Newton method: Find a Newton update $\tilde{\mathbf{v}}$ and $\tilde{\boldsymbol{\pi}}$ such that

$$(\rho_{\text{ice}} H^{n+1} \tilde{\mathbf{v}}, \phi) + \delta t B'(\mathbf{v}_l, \boldsymbol{\pi}_l)(\tilde{\mathbf{v}}, \tilde{\boldsymbol{\pi}}, \phi) - \delta t \tau'_{\text{ocean}}(\mathbf{v}_l)(\tilde{\mathbf{v}}, \phi) = F(\phi) - (\rho_{\text{ice}} H^{n+1} \mathbf{v}_l, \phi) - \delta t B(\mathbf{v}_l, \boldsymbol{\pi}_l, \phi) + \delta t \tau_{\text{ocean}}(\mathbf{v}_l) \quad (17a)$$

$$\mathbf{r}'(\boldsymbol{\pi}_l, \mathbf{v}_l)(\tilde{\boldsymbol{\pi}}, \tilde{\mathbf{v}}) = -\mathbf{r}(\boldsymbol{\pi}_l, \mathbf{v}_l) \quad (17b)$$

for all $\phi \in V$, and then perform the Newton update step $\mathbf{v}_{l+1} := \mathbf{v}_l + \alpha \tilde{\mathbf{v}}$ and $\boldsymbol{\pi}_{l+1} := \boldsymbol{\pi}_l + \alpha \tilde{\boldsymbol{\pi}}$ with a step length $\alpha \leq 1$.

The Gateaux derivative $\mathbf{r}'(\boldsymbol{\pi}, \mathbf{v})$ with respect to \mathbf{v} and $\boldsymbol{\pi}$ can be computed as follows:

$$\mathbf{r}'(\boldsymbol{\pi}, \mathbf{v})(\tilde{\boldsymbol{\pi}}, \tilde{\mathbf{v}}) = \tilde{\boldsymbol{\pi}} \Delta(\mathbf{v}) + \frac{2\boldsymbol{\tau}(\tilde{\mathbf{v}}) : \boldsymbol{\tau}(\mathbf{v})}{\Delta(\mathbf{v})} \boldsymbol{\pi} - \boldsymbol{\tau}(\tilde{\mathbf{v}}) = \tilde{\boldsymbol{\pi}} \Delta(\mathbf{v}) + \frac{2\boldsymbol{\tau}(\mathbf{v}) \otimes \boldsymbol{\pi}}{\Delta(\mathbf{v})} \boldsymbol{\tau}(\tilde{\mathbf{v}}) - \boldsymbol{\tau}(\tilde{\mathbf{v}}). \quad (18)$$

Thus, the Newton step (17b) is

$$\tilde{\boldsymbol{\pi}} \Delta(\mathbf{v}_l) + \frac{2\boldsymbol{\tau}(\mathbf{v}_l) \otimes \boldsymbol{\pi}_l}{\Delta(\mathbf{v}_l)} \boldsymbol{\tau}(\tilde{\mathbf{v}}) - \boldsymbol{\tau}(\tilde{\mathbf{v}}) = -\boldsymbol{\pi}_l \Delta(\mathbf{v}_l) + \boldsymbol{\tau}(\mathbf{v}_l). \quad (19)$$

Computing the remaining derivative terms in (18) is straightforward. Namely, $B'(\mathbf{v}, \boldsymbol{\pi})(\tilde{\mathbf{v}}, \tilde{\boldsymbol{\pi}}, \phi) = (P^{n+1} \tilde{\boldsymbol{\pi}}, \tau(\phi))$ and τ'_{ocean} is computed in (12b).

Next, as in [43], we eliminate (17b) from the system. Dividing the Newton step (19) by $\Delta(\mathbf{v}_l)$ shows that

$$\tilde{\boldsymbol{\pi}} = -\boldsymbol{\pi}_l + \frac{\boldsymbol{\tau}(\mathbf{v}_l)}{\Delta(\mathbf{v}_l)} + \frac{\boldsymbol{\tau}(\tilde{\mathbf{v}})}{\Delta(\mathbf{v}_l)} - \frac{2\boldsymbol{\tau}(\mathbf{v}_l) \otimes \boldsymbol{\pi}_l}{\Delta(\mathbf{v}_l)^2} \boldsymbol{\tau}(\tilde{\mathbf{v}}). \quad (20)$$

Using this in (18), we find the following linear equation for $\tilde{\mathbf{v}}$:

$$\begin{aligned} (\rho_{\text{ice}} H^{n+1} \tilde{\mathbf{v}}, \phi) + \delta t \left(\frac{P^{n+1}}{\Delta(\mathbf{v}_l)} \boldsymbol{\tau}(\tilde{\mathbf{v}}), \boldsymbol{\tau}(\phi) \right) - \delta t \left(2P^{n+1} \frac{\boldsymbol{\tau}(\mathbf{v}_l) \otimes \boldsymbol{\pi}_l}{\Delta(\mathbf{v}_l)^2} \boldsymbol{\tau}(\tilde{\mathbf{v}}), \boldsymbol{\tau}(\phi) \right) - \delta t \boldsymbol{\tau}'_{\text{ocean}}(\mathbf{v}_l)(\tilde{\mathbf{v}}, \phi) \\ = F(\phi) - (\rho_{\text{ice}} H^{n+1} \mathbf{v}_l, \phi) - \delta t \left(\frac{P^{n+1}}{\Delta(\mathbf{v}_l)} \boldsymbol{\tau}(\mathbf{v}_l), \boldsymbol{\tau}(\phi) \right) + \delta t \left(\frac{P^{n+1}}{2}, \text{tr}(\dot{\boldsymbol{\varepsilon}}(\phi)) \right) + \delta t \boldsymbol{\tau}_{\text{ocean}}(\mathbf{v}_l). \end{aligned} \quad (21)$$

Note that the right hand side in the above system coincides with the right hand side in the original Newton method (12a). The left hand side is similar to the one in (12a), with the difference that $\boldsymbol{\tau}(\mathbf{v})/\Delta(\mathbf{v}_l)$ in the second term of (12a) is replaced by $\boldsymbol{\pi}_l$ in (21). Having solved (21) for the Newton step $\tilde{\mathbf{v}}$, we use (20) to compute the Newton step for $\boldsymbol{\pi}$, which involves a matrix vector multiplication and does not require solving a linear system.

On top of the above derivation, analogously as in [43], we enforce that the 4th-order tensor in (21) is symmetric and that $\sqrt{2}\boldsymbol{\pi}_l$ remains in the unit sphere by replacing

$$\boldsymbol{\tau}(\mathbf{v}_l) \otimes \boldsymbol{\pi}_l \quad \text{by} \quad \frac{\boldsymbol{\tau}(\mathbf{v}_l) \otimes \boldsymbol{\pi}_l + \boldsymbol{\pi}_l \otimes \boldsymbol{\tau}(\mathbf{v}_l)}{2 \max(1, \sqrt{2\boldsymbol{\pi}_l : \boldsymbol{\pi}_l})}. \quad (22)$$

The same modifications are applied to the last term in (20) for consistency. We note that both modifications vanish upon convergence. First, upon convergence, i.e., $\boldsymbol{\pi}$ satisfies (13), $\boldsymbol{\pi}$ is a multiple of $\boldsymbol{\tau}$ and thus symmetric so the symmetrization has no or very little effect when close to the solution. Second, upon convergence, $\sqrt{\boldsymbol{\pi}_l : \boldsymbol{\pi}_l} \leq 1/\sqrt{2}$ and thus the scaling has no effect.

5. Numerical Results

In this section, we compare the convergence behavior of various Newton-type methods and implementations for two test problems. The first problem (Section 5.2) is a challenging single time step problem for the momentum equation. The second problem (Section 5.3) is a benchmark from [34], which includes the evolution of sea-ice concentration A and sea-ice thickness H . Both problems use the physical parameters summarized in Table 1. In particular, we assume that there is no Coriolis force and thus $f_c = 0$. Finally, in Section 5.4, we propose and study iterative solvers for the linearized systems arising in each Newton step.

5.1. Methods and implementations

We compare the performance of various Newton-type methods, including the proposed stress-velocity Newton method (denoted as “svN. (Firedrake)”), a standard Newton method (denoted as “stdN. (Firedrake)”), a modified Newton method from [36] implemented in the academic software library GASCOIGNE 3D [6] (denoted as “modN. (Gascoigne)”), and a Jacobian-free Newton-Krylov (JFNK) solver [30, 32] from the MITGCM library [2] (denoted as “JFNK (MITgcm)”). For details about these solvers, we refer to the literature above. Our comparisons with modN. (Gascoigne) and JFNK (MITgcm) are only in terms of the Newton iterations and thus implementation and discretizations aspects play a limited role. All implementations use the same smooth transition between the viscous and plastic regime specified in (3). In our own implementation, we additionally compare the performance of various solvers for the linearized systems and report timings and parallel scalability results in Section 5.4.

Our implementations of the standard Newton method and the stress-velocity Newton methods² are based on the open source finite element library Firedrake [1, 11, 16, 37, 39] and its interface with the parallel linear algebra toolkit PETSC [4, 5]. We use structured quadrilateral meshes to discretize the spatial domain Ω . Unless otherwise specified, we use linear \mathbb{Q}_1 elements to discretize the sea-ice velocity \mathbf{v} . Finite volumes are used for the sea-ice concentration A and thickness H , i.e., $\mathbb{Q}_0^{\text{disc}}$ elements. Our implementation (and the proposed method) also allows to use higher-order discretizations, and we show

²Source codes are available at https://github.com/MelodyShih/SeaIce_svNewton.

Parameter	Definition	Value
ρ_{ice}	sea-ice density	900 kg/m ³
ρ_{a}	air density	1.3 kg/m ³
ρ_{o}	water density	1026 kg/m ³
C_{a}	air drag coefficient	1.2×10^{-3}
C_{o}	water drag coefficient	5.5×10^{-3}
P^*	ice strength parameter	27.5 N/m ²
C	ice concentration parameter	20
e	ellipse ratio	2
f_c	Coriolis parameter	0

Table 1: Physics parameters used in the momentum equation for both test problems.

results obtained with quadratic finite elements in space for the problem discussed in Section 5.3. We terminate the nonlinear iteration when we obtain 10^4 reduction in the L_2 -norm of the nonlinear residual $\|A(\mathbf{v}_l, \phi) - F(\phi)\|_2$. To compute a step length for the Newton updates $\tilde{\mathbf{v}}$ (and $\tilde{\pi}$), we use backtracking with the optimization objective (6), starting from unit step length and halving the step length if the objective does not decrease. Using the norm of the nonlinear residual rather than the optimization objective for backtracking results in similar results. We either use the parallel direct sparse solver MUMPS [3] to solve the linearized problems arising in each Newton step, or an iterative parallel Krylov solver, which we detail in Section 5.4.

5.2. Problem I: Single momentum equation solve

This is a challenging single momentum solve problem due to the severe nonlinearity of the constitutive relation. We consider the square domain $\Omega = (0, 512 \text{ km})^2$. The atmospheric and ocean forcing are constant in space and time and are given by $\mathbf{v}_o(\mathbf{x}) = \mathbf{0} \text{ ms}^{-1}$ and $\mathbf{v}_a(\mathbf{x}) = (5, 5) \text{ ms}^{-1}$, and we consider a sea-ice concentration A and the thickness H given by

$$A(\mathbf{x}) := 1 - 0.5e^{-800|r(\mathbf{x})|} - 0.4e^{-90|r_1(\mathbf{x})|} - 0.4e^{-90|r_1(\mathbf{x})+0.7|} \quad \text{and} \quad H(\mathbf{x}) := 2A(\mathbf{x}),$$

where

$$\begin{aligned} r(\mathbf{x}) &= r(x, y) = 0.04 - \left(\frac{x}{1000 \text{ km}} - 0.25\right)^2 - \left(\frac{y}{1000 \text{ km}} - 0.25\right)^2, \\ r_1(\mathbf{x}) &= r_1(x, y) = 0.1 + \left(\frac{2x}{1000 \text{ km}}\right)^2 - \left(\frac{2y}{1000 \text{ km}}\right). \end{aligned}$$

These sea-ice concentration and thickness field have narrow regions where they are reduced, as shown in the top left of Figure 1. The initial velocity is $\mathbf{v}(0, \mathbf{x}) = \mathbf{0} \text{ ms}^{-1}$ and we assume zero Dirichlet boundary conditions for the velocity \mathbf{v} . We use a time step size of $\delta t = 0.5 \text{ h}$ for the first (and only) time step, and unless otherwise specified, a spatial mesh size of $\Delta x = \Delta y = 1 \text{ km}$, and $\Delta_{\min} = 2 \times 10^{-9}$. The sea-ice velocity solution \mathbf{v} is shown in the top right of Figure 1. Next, we compare the performance of various solvers.

The bottom figure in Figure 1 compares the nonlinear convergence of various solvers. We observe a significant reduction in the number of Newton iterations of the proposed method **svN. (Firedrake)** compared to the standard Newton method **stdN. (Firedrake)**. The **stdN. (Firedrake)** makes little progress within 200 iterations, while the **svN. (Firedrake)** is able to reduce the residual by a factor of 10^4 in 30 iterations. In addition, the **svN. (Firedrake)** outperforms the other two methods: in terms of the number of iterations, it converges 2.6 times faster than the **modN. (Gascoigne)**, and about 7 times faster than the **JFNK (MITgcm)**. As will be shown in the next section, the difference in Newton iterations becomes even larger with higher grid resolution. In the table in Figure 1, we also show that the number of Newton iterations only increases moderately upon mesh refinement, increasing from 30 for $\Delta x = 1 \text{ km}$ to 37 for $\Delta x = 0.5 \text{ km}$ and to 45 for $\Delta x = 0.25 \text{ km}$.

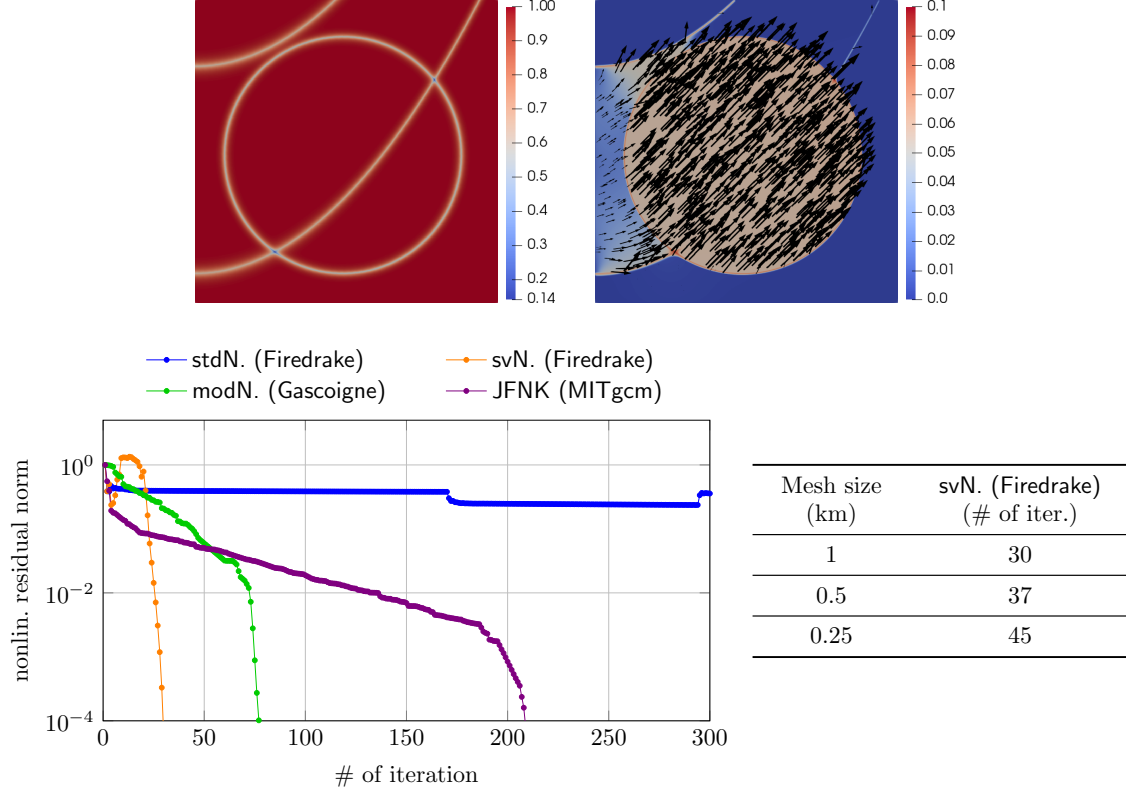


Figure 1: Setup and convergence for Problem I. The top left image shows the concentration field A , which has narrow regions with reduced concentration. The ice height H is a constant multiple of A . The top right figure shows the computed sea-ice velocity \mathbf{v} . Arrows show the velocity direction and the background color depicts the velocity magnitude, which has sharp gradients as a result of the viscous-plastic constitutive relation. Shown at the bottom left is the L_2 -norm of the nonlinear residual in each iteration for various methods and implementations with mesh size $\Delta x = 1$ km. On the bottom right, we show the number of iterations of svN. (Firedrake) for two finer mesh sizes $\Delta x = 0.5$ km, 0.25 km.

5.3. Problem II: Time-dependent sea-ice benchmark from [34]

In this test problem, we solve the full time dependent equations (1) for the benchmark problem from [34]. In particular, we use the following parameters and forcing. We consider a square domain $\Omega = (0, 512 \text{ km})^2$ and the atmospheric velocity \mathbf{v}_a and the ocean flow velocity \mathbf{v}_o in (5) are

$$\mathbf{v}_o(t, x, y) = 0.01 \text{ ms}^{-1} \begin{pmatrix} -1 + 2y/(512 \text{ km}) \\ 1 - 2x/(512 \text{ km}) \end{pmatrix},$$

$$\mathbf{v}_a(t, x, y) = \omega(x, y) \bar{\mathbf{v}}_a^{\max} \begin{pmatrix} \cos(\alpha) & \sin(\alpha) \\ -\sin(\alpha) & \cos(\alpha) \end{pmatrix} \begin{pmatrix} x - m_x(t) \\ y - m_y(t) \end{pmatrix},$$

where

$$\bar{\mathbf{v}}_a^{\max} = \bar{\mathbf{v}}_a^{\max}(t) = 15 \text{ ms}^{-1} \begin{cases} -\tanh((4-t)(4+t)/2) & t \in [0, 4] \text{ d} \\ \tanh((12-t)(-4+t)/2) & t \in [4, 8] \text{ d} \end{cases},$$

$$\alpha = \alpha(t) = \begin{cases} 72^\circ & t \in [0, 4] \text{ d} \\ 81^\circ & t \in [4, 8] \text{ d} \end{cases},$$

$$m_x(t) = m_y(t) = \begin{cases} 256 \text{ km} + 51.2 \text{ km/d} \cdot t & t \in [0, 4] \text{ d} \\ 665.6 \text{ km} - 51.2 \text{ km/d} \cdot t & t \in [4, 8] \text{ d} \end{cases}$$

$$\omega(x, y) = \omega(t, x, y) = \frac{1}{50} \exp \left(-\frac{\sqrt{(x - m_x(t))^2 + (y - m_y(t))^2}}{100 \text{ km}} \right).$$

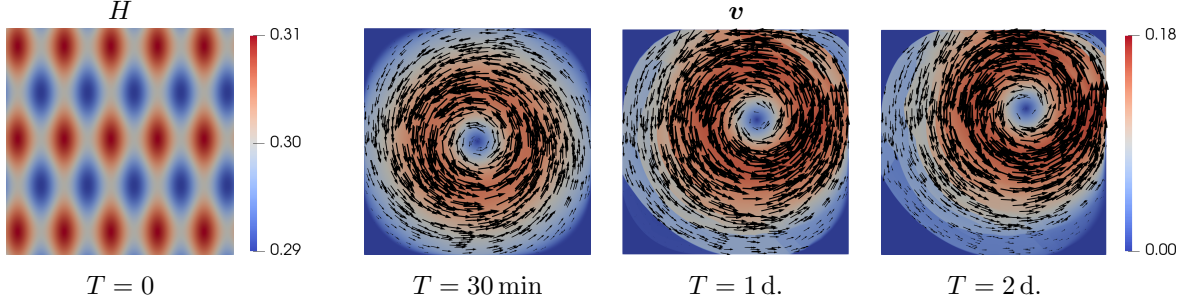


Figure 2: Initial ice height H and sea-ice velocity \mathbf{v} (ms^{-1}) at different times T for Problem II. Arrows in the right three plots show the direction of the velocity field and the colors depict its magnitude. Note the discontinuities in the sea-ice velocity magnitude, which are due to the nonlinear rheology. Results are from a run on a quadrilateral mesh with mesh size $\Delta x = \Delta y = 2$ km using **svN**. (**Firedrake**).

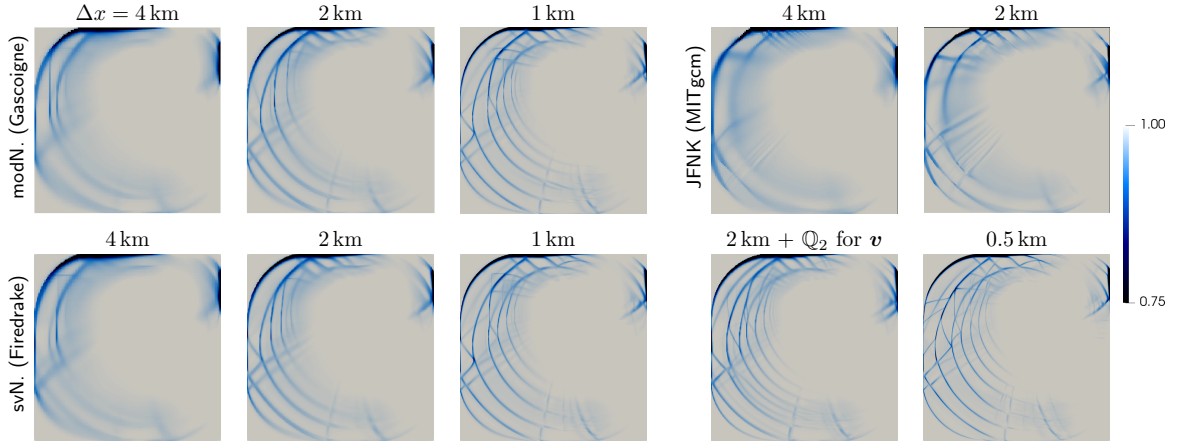


Figure 3: Sea ice concentration A at 2 days for Problem II computed with different mesh resolutions and methods. All simulations use a 0.5 h time step and thus $48 \text{ h}/0.5 \text{ h} = 96$ time steps. For the run with \mathbb{Q}_2 for \mathbf{v} , we use $\mathbb{Q}_1^{\text{disc}}$ for A and H .

As initial conditions, we use

$$\mathbf{v}(0, \mathbf{x}) = \mathbf{0} \text{ ms}^{-1}, \quad A(0, \mathbf{x}) = 1, \quad H(0, x, y) = 0.3 \text{ m} + 0.005 \text{ m} \left(\sin \left(\frac{60x}{1000 \text{ km}} \right) + \sin \left(\frac{30y}{1000 \text{ km}} \right) \right).$$

We use the time step size $\delta t = 0.5 \text{ h}$ for all our simulations and unless otherwise specified, $\Delta_{\min} = 2 \times 10^{-9}$. The resulting velocity field, sea-ice concentration and shear deformation are shown in Figures 2 to 4. Note that the simulations yield more small-scale solution features on finer meshes. The results obtained with the **modN**. (**Gascoigne**) implementation largely coincides with our solution on the corresponding meshes. To illustrate that the method does not rely on a specific discretization, we also show a result with quadratic elements for sea-ice velocity \mathbf{v} on a 2 km mesh. This discretization has the same number of velocity unknowns as the linear element discretization for \mathbf{v} on the 1 km mesh, and the solutions are similar. Higher-order spatial discretization are unlikely to result in substantially more accurate solutions as the fields typically have large variations of gradients due to the constitutive relation. The **JFNK** (**MITgcm**) solutions are slightly different. Similar differences between solutions obtained with different discretization have also been observed in the benchmark study [34].

Nonlinear solver convergence. Figure 5 and Table 2 compare the performance of different methods for the benchmark problem using a 4 km and a 2 km mesh discretization. In particular, in Figure 5, we show the number of Newton iterations required for each time step, and in Table 2, we show the number of average Newton iterations over all time steps. In this table, we also include a run with the smaller

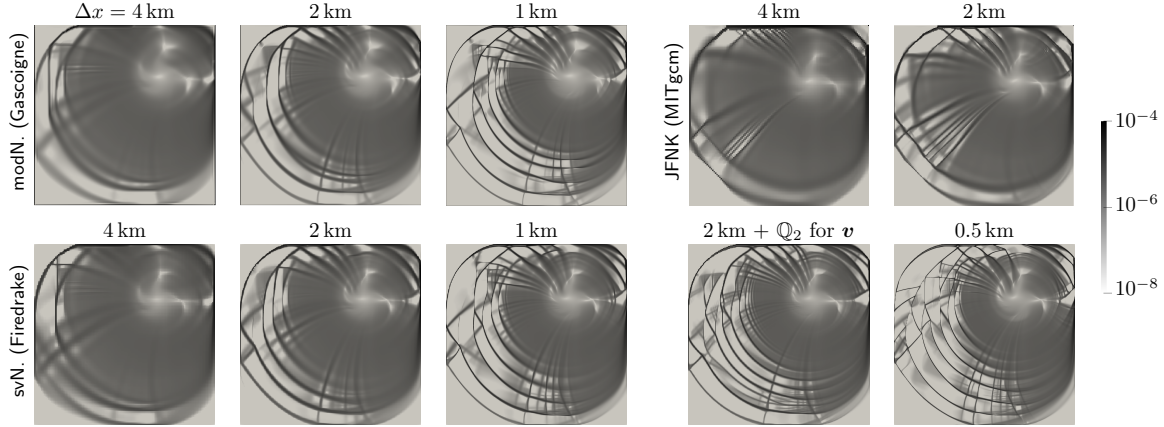


Figure 4: Shear deformation $2\sqrt{-\det \tilde{\epsilon}'}$ after 2 days (96 time steps) for Problem II.

Table 2: Average number of Newton iterations over an 4-day simulation of Problem II. The number of time steps, i.e., the total number of the nonlinear solves for all runs is 384. A dash indicates that the run failed, i.e., for at least one time step, the nonlinear solver did not converge after 200 iterations.

Δ_{\min}	2×10^{-9}				2×10^{-10}
Mesh size	4 km	2 km	1 km	0.5 km	4 km
stdN. (Firedrake)	52.75	78.77	162.21	—	—
svN. (Firedrake)	6.66	11.32	15.91	20.20	10.15
modN. (Gascoigne)	10.35	15.87	26.51	N/A	—
JFNK (MITgcm)	21.34	—	N/A	N/A	N/A

$\Delta_{\min} = 2 \times 10^{-10}$, the constant that prevents division by zero in (10), for which only the svN. (Firedrake) converges. These results highlight the robustness of the svN. (Firedrake), whose average number of iterations is more robust to mesh refinement and the parameter Δ_{\min} . Convergence failures, i.e., no reduction of the nonlinear residual by 4 orders of magnitude after 200 iterations, occur for stdN. (Firedrake) when we refine the mesh and/or use a smaller Δ_{\min} . A similar behavior is observed for JFNK (MITgcm) for the smaller mesh discretization. The modN. (Gascoigne) performs comparably with the svN. (Firedrake), except between day 4 and 5, which is when the atmospheric velocity v_a changes its direction, making the problem particularly difficult to solve. It however fails when $\Delta_{\min} = 2 \times 10^{-10}$.

5.4. Iterative solution of linearized systems

Sea-ice simulations can easily have millions of spatial unknowns, and thus it might be infeasible to use direct solvers for the linearized systems arising in each Newton step. Several iterative approaches, typically preconditioned Krylov methods, have been proposed to solve the arising linear systems. For instance, a line successive over-relaxation method (LSOR) as preconditioner is proposed in the context of a Jacobian-free Newton-Krylov solver in [30]. In [32], the authors suggest to replace the computationally expensive LSOR preconditioner by an incomplete LU-factorization (ILU) preconditioner, in particular for high spatial resolutions. The performance of a geometrical multigrid (GMG) method as a preconditioner is compared to an ILU preconditioner in [35]. Multigrid preconditioning is shown to substantially reduce the computational cost and decreased iteration counts by 80% compared to the ILU preconditioner. However, GMG requires a hierarchy of meshes, which is in general not available in climate simulations. This motivates the use of algebraic multigrid (AMG) preconditioners, which we discuss next.

Note that each Newton linearization of the momentum equation is a symmetric elliptic vector system with strongly varying and anisotropic coefficients, which are a result of the severe nonlinearity of the constitutive relation. For the standard Newton linearization, symmetry and positive-definiteness has been

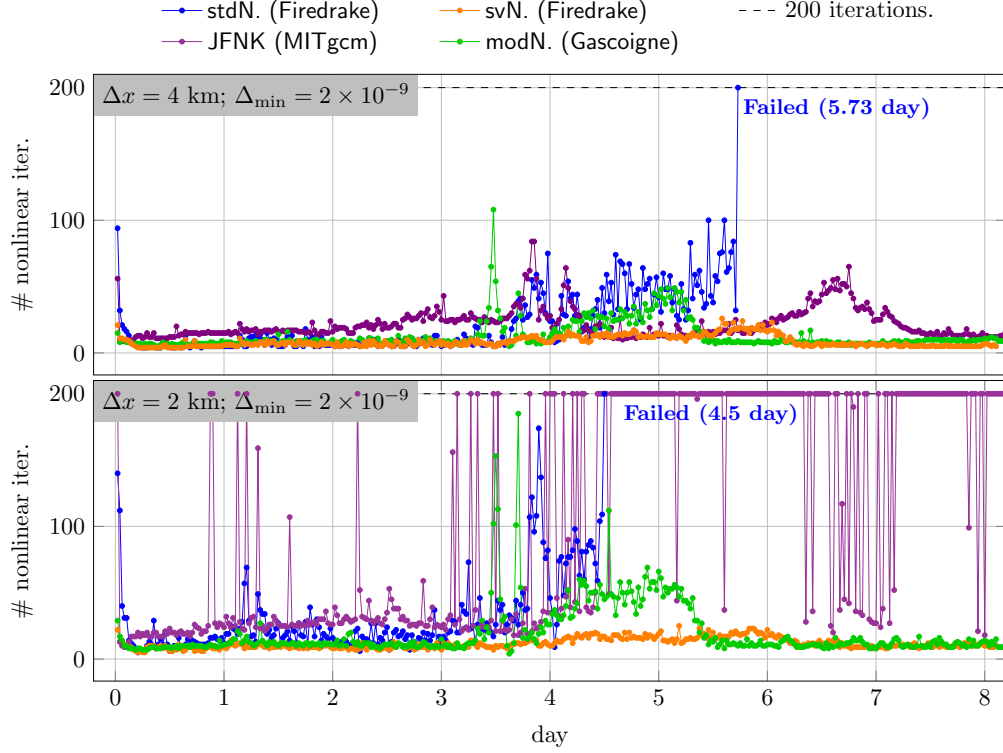


Figure 5: Convergence behavior of different Newton-type solvers for Problem II with mesh sizes $\Delta x = 4$ km and $\Delta x = 2$ km. Shown is the number of Newton iterations to reduce the nonlinear residual by a factor of 10^4 at each time step. For data from JFNK (MITgcm), the simulation continues even when the residual is not sufficiently decreased after 200 iterations.

shown in [36] by reformulating the momentum equation to (12) and follows directly from the underlying energy minimization formulation (6). For the stress-velocity Newton method, symmetry and ellipticity are not automatically satisfied due to the introduction of the variable π . Hence, positive-definiteness and symmetry of the linearization are enforced through the modification of the Jacobian given in (22). This makes the system suitable for iterative solvers that have been successfully used for elliptic systems, such as AMG.

In particular, we use the flexible generalized minimum residual (FGMRES) method, preconditioned with AMG. As AMG implementation, we use the parallel implementation BoomerAMG [44] through PETSc's interface to Hypre [14]. We mostly use default parameters in BoomerAMG including a symmetric successive over-relaxation smoother, Gaussian elimination on the coarsest level, Falgout coarsening and a V-cycle. However, we made two changes that are necessary due to the strongly varying coefficients, namely we choose 3 smoothing steps on each level and we set the strong threshold to 0.5 (compared to the usual value of 0.25 for two-dimensional problems). The latter choice results in a smaller number of nonzero entries for the coarser AMG matrices. The reduced fill-in helps control the operator complexity and results in faster V-cycles without degrading the preconditioning performance.

On the left of Figure 6, we show the number of Krylov iterations required to solve the (stress-velocity) Newton linearizations arising in the momentum equation at the first time step of Problem II. We either use AMG or an ILU preconditioner and show results for various mesh resolutions Δx . We find that on the coarsest mesh, i.e., $\Delta x = 4$ km, the two preconditioners behave similarly. On finer meshes, AMG outperforms the ILU preconditioner significantly. In fact, FGMRES with ILU preconditioning fails to converge within 300 iterations for meshes with resolution higher than 4 km (not all shown in the figure). Note that the preconditioning performance of ILU could possibly be improved by reordering the unknowns. The number of Krylov iterations needed when using the AMG preconditioner increases moderately when we refine the mesh. The same behavior has been observed by using a GMG preconditioner in [35]. Such an

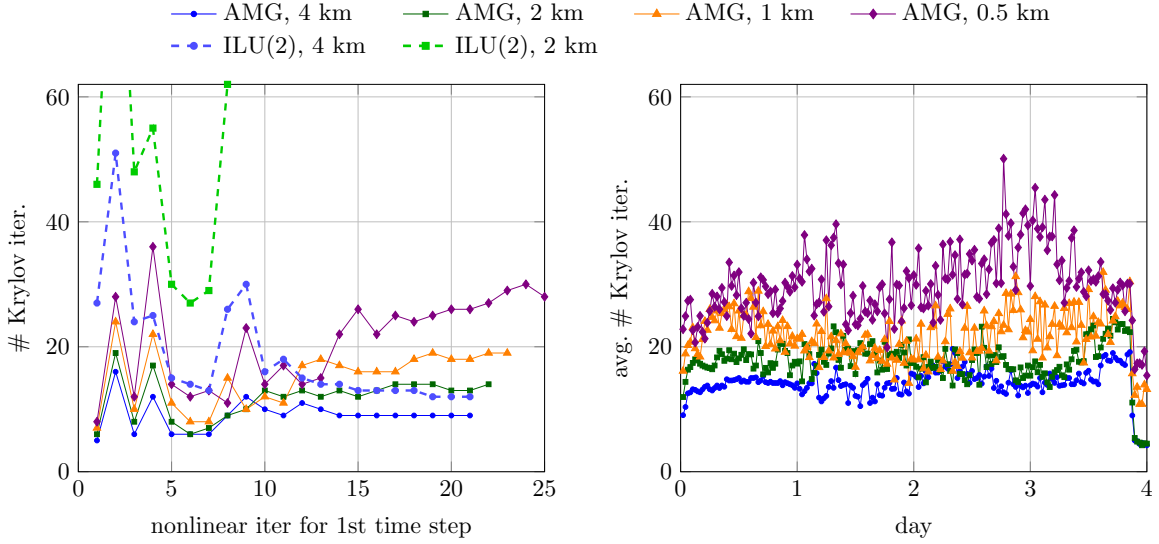


Figure 6: Convergence of preconditioned Krylov method for linearized systems for Problem II. Shown on the left is the number of preconditioned Krylov iterations (y -axis) required for each Newton linearization (x -axis) for the first time step. Shown are results for differently mesh sizes Δx using an AMG or an incomplete LU preconditioner. Shown on the right is the number of average Krylov iterations preconditioned with AMG needed for the linear Newton solves at each time step. Note that the number of Krylov iterations varies but remains moderate for all Newton linearizations throughout the 4-day simulation. On average, 14, 17, 22 and 30 Krylov iterations are needed for the meshes with $\Delta x = 4\text{km}, 2\text{km}, 1\text{km}, 0.5\text{km}$, respectively.

increase is typically not observed for multigrid preconditioners for simpler elliptic problems. The reason for the behavior here is that upon mesh refinement, the VP constitutive relation leads to smaller-scale features and thus steeper gradients in the solution fields as can be seen from Figure 4. Thus, finer discretizations resolve the nonlinearity better and thus the linear systems become harder to solve.

To show that the behavior we observe for the first time step is representative for later time steps, the right plot in Figure 6 shows the average number of AMG-preconditioned Krylov iterations for each linear solve for all time steps for a simulation up to day 4. Note that the AMG-preconditioned Krylov solver converges robustly for all time steps and all linear systems arising from the stress-velocity Newton linearization. We again observe that this average number is moderately larger on finer meshes, most likely due to the more complex behavior that is resolved on finer meshes, which makes the resulting systems more ill-conditioned.

Finally, we study the weak parallel scalability of our solver and present a comparison of timings in Figure 7. In a weak scaling study, one increases the problem size (by refining the mesh) and, at the same time, increases the computational resources used for solving the problem. When this is done such that the computational work per compute core remains roughly the same, perfect weak scalability would amount to constant run time. As baseline, we show the time for the first momentum solve based on the standard Newton linearization with line search and the direct parallel solver MUMPS [3] in Figure 7 (blue bars). Since MUMPS's (and any direct solver's) parallel scalability is limited, we do not go beyond one compute node, i.e., the 56 CPU cores that share the same physical memory. The substantial growth in runtime we observe as we go from a 4 km to a 0.25 km mesh is primarily due to the increasing number of Newton steps upon mesh refinement. Using the proposed alternative Newton linearization results in a substantial improvement due to a much more moderate increase in the number of Newton iterations and resulting wall time (green bars). For instance, from Table 2 we observe that the number of Newton iteration increases from 16 for $\Delta x = 1\text{ km}$ to 20 for $\Delta x = 0.5\text{ km}$. The growth in run time is more significant, however, due to the limited weak parallel scalability of direct solvers. Finally, we combine the proposed Newton linearization with the AMG-preconditioned Krylov method to solve the linear problems (orange bars). First, we observe a significant reduction in overall run time. The remaining growth going

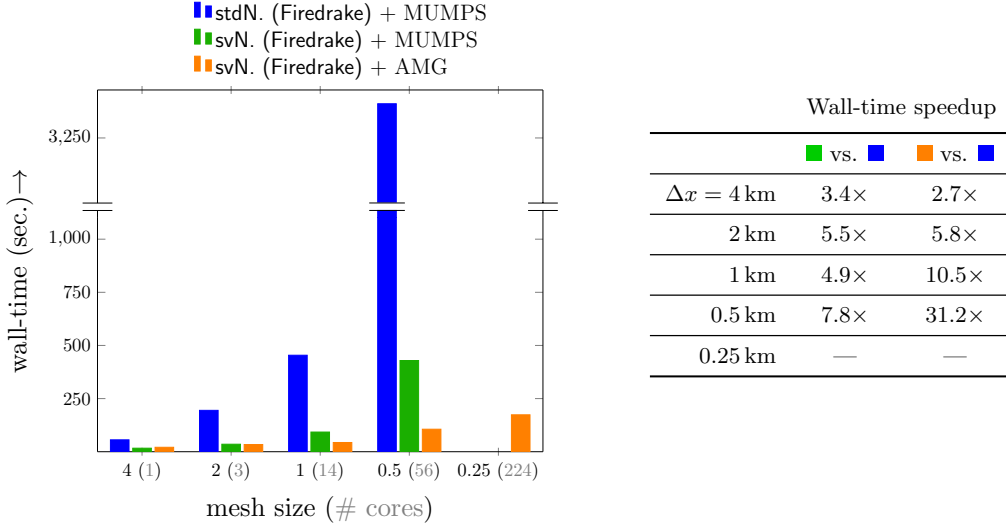


Figure 7: Weak scalability on Texas Advanced Computing Center’s Frontera (Intel Cascade Lake nodes) for first momentum solve in Problem II. Shown on the left are the wall clock times for a weak parallel scaling study. Shown in brackets is the number of Message Passing Interface (MPI) processes chosen so that the number of unknowns per core are around 32K. Timings for three implementations are compared, namely a standard Newton method (blue) and the proposed velocity-stress Newton method (green), both using the direct linear solver MUMPS [3]. Shown in orange are timings for the velocity-stress Newton method with an AMG-preconditioned Krylov method as iterative linear solver. For mesh resolution of 0.25 km, only the solver proposed in this paper can be used as the problem has 8.4 million unknowns. The table on the right compares the speedup factors for the different methods.

from coarse to fine meshes is mainly due to the increasing number of Krylov iterations when the mesh is refined (compare the left plot in Figure 6). This increase is larger for the first momentum solve than on average as can be seen on the right plot in Figure 6, where we find that the average number of Krylov iterations goes up by a factor of ≈ 2 comparing $\Delta x = 4$ km with $\Delta x = 0.5$ km. Hence, on average, we expect a more favorable scalability of our stress-velocity Newton linearization with AMG-preconditioned Krylov solver than shown in Figure 7. An additional factor contributing to the increase in solve time is the required Message Passing Interface communication through the network due to parallelism.

6. Conclusion

We have shown that a novel linearization of the momentum equation arising in the commonly used VP sea-ice model results in faster and more robust Newton convergence, with iteration numbers that only increase moderately upon mesh refinement (see the table in Figure 1 and Table 2). The approach is motivated by the observation that the implicit time step of the momentum equation can also be written as an energy minimization problem. This suggested the alternative Newton linearization presented here, which is similar to techniques used in primal-dual optimization algorithms. We hope that these ideas will eventually be adopted in the sea-ice community as they substantially reduce the computational cost for implicitly time-stepped VP models and thus enable finer mesh resolutions and better resolved models. More generally, the approach to lift nonlinear equations to a higher dimensional space before Newton linearization could be useful for other challenging systems as well.

Note that our derivation of the alternative Newton step assumes an elliptic yield curve, i.e., the most common yield criterion for viscous-plastic sea-ice models. Other yield curves are possible and scientifically relevant (e.g., [42, 50]) and it remains to be seen if our approach generalizes to these different constitutive relationships.

We additionally study iterative parallel solvers for the large and ill-conditioned (but positive definite) systems arising upon Newton linearizations. We propose and study AMG as preconditioner for a Krylov method to solve these systems. Computational efficiency is a strong constraint for sea-ice models in the

climate modeling context. Any new method will need to demonstrate that it can meet this requirement so that accurate sea ice dynamics solutions become available at reasonable cost. The computational cost of the primal-dual Newton-Krylov solver with AMG preconditioning increases only moderately with grid refinement. Further, AMG does not require a mesh hierarchy and efficient parallel open-source AMG libraries are available, so that this combination of methods may be a good candidate for solving the momentum equation of sea-ice models in particular, and for climate simulations in general.

Acknowledgements

This work has been supported by the Multidisciplinary University Research Initiatives (MURI) Program, Office of Naval Research (ONR) grant number N00014-19-1-2421, and by the DFG priority program “Antarctic Research with Comparative Investigations in Arctic Ice Areas” project number 463061012.

References

- [1] Acosta, G., Apel, T., Duran, R., Lombardi, A., 2011. Error estimates for Raviart-Thomas interpolation of any order on anisotropic tetrahedra. *Math. Comput.* 80, 141–163.
- [2] Adcroft, A., Campin, J., Dutkiewicz, S., Evangelinos, C., D. Ferreira, D., Forget, G., Fox-Kemper, B., Heimbach, P., Hill, C., Hill, E., Hill, H., Jahn, O., Losch, M., Marshall, J., Maze, G., Menemenlis, D., Molod, A., 2018. MITgcm User Manual.
- [3] Amestoy, P.R., Duff, I.S., L’Excellent, J.Y., Koster, J., 2001. A fully asynchronous multifrontal solver using distributed dynamic scheduling. *SIAM Journal on Matrix Analysis and Applications* 23, 15–41.
- [4] Balay, S., Abhyankar, S., Adams, M.F., Brown, J., Brune, P., Buschelman, K., Dalcin, L., Eijkhout, V., Gropp, W.D., Karpeyev, D., Kaushik, D., Knepley, M.G., May, D.A., McInnes, L.C., Mills, R.T., Munson, T., Rupp, K., Sanan, P., Smith, B.F., Zampini, S., Zhang, H., Zhang, H., 2019. PETSc Users Manual. Technical Report ANL-95/11 - Revision 3.11. Argonne National Laboratory.
- [5] Balay, S., Gropp, W.D., McInnes, L.C., Smith, B.F., 1997. Efficient management of parallelism in object oriented numerical software libraries, in: Arge, E., Bruaset, A.M., Langtangen, H.P. (Eds.), *Modern Software Tools in Scientific Computing*, Birkhäuser Press. pp. 163–202.
- [6] Becker, R., Braack, M., Meidner, D., Richter, T., Vexler, B., 2021. The finite element toolkit GASCOIGNE 3D. <https://www.gascoigne.de>.
- [7] Blockley, E., Vancoppenolle, M., Hunke, E.C., Bitz, C., Feltham, D.L., Lemieux, J.F., Losch, M., Maisonnave, E., Notz, D., Rampal, P., Tietsche, S., Tremblay, B., Turner, A., Massonnet, F., Ólason, E., Roberts, A., Aksenov, Y., Fichefet, T., Garric, G., Iovino, D., Madec, G., Rousset, C., Salas y Melia, D., Schroeder, D., 2020. The Future of Sea Ice Modeling: Where Do We Go from Here? *Bulletin of the American Meteorological Society* 101, 1304–1311.
- [8] Bouillon, S., Fichefet, T., Legat, V., Madec, G., 2013. The elastic-viscous-plastic method revisited. *Ocean Modelling* 71, 2–12.
- [9] Brandt, F., Disser, K., Haller-Dintelmann, R., Hieber, M., 2021. Rigorous analysis and dynamics of Hibler’s sea ice model. *arXiv:2104.01336*.
- [10] Chan, T.F., Golub, G.H., Mulet, P., 1999. A nonlinear primal-dual method for total variation-based image restoration. *SIAM Journal on Scientific Computing* 20, 1964–1977. URL: <https://doi.org/10.1137/S1064827596299767>, doi:10.1137/S1064827596299767.
- [11] Dalcin, L.D., Paz, R.R., Kler, P.A., Cosimo, A., 2011. Parallel distributed computing using Python. *Advances in Water Resources* 34, 1124–1139. doi:<http://dx.doi.org/10.1016/j.advwatres.2011.04.013>. new Computational Methods and Software Tools.

- [12] Damsgaard, A., Adcroft, A., Sergienko, O., 2018. Application of discrete element methods to approximate sea ice dynamics. *Journal of Advances in Modeling Earth Systems* 10, 2228–2244.
- [13] Danilov, S., Mehlmann, C., Fofonova, V., 2022. On discretizing sea-ice dynamics on triangular meshes using vertex, cell or edge velocities. *Ocean Modelling* 170, 101937.
- [14] Falgout, R., Yang, U., 2002. hypre: A library of high performance preconditioners. *Computational Science-ICCS 2002, Pt Iii, Proceedings* 2331, 632–641. doi:10.1007/3-540-47789-6_66.
- [15] Girard, L., Bouillon, S., Weiss, J., Amitrano, D., Fichefet, T., Thierry, L., Legat, V., 2011. A new modeling framework for sea-ice mechanics based on elasto-brittle rheology. *Annals of Glaciology* 52, 123–132.
- [16] Hendrickson, B., Leland, R., 1995. A multilevel algorithm for partitioning graphs, in: *Supercomputing '95: Proceedings of the 1995 ACM/IEEE Conference on Supercomputing (CDROM)*, ACM Press, New York. p. 28. doi:<https://doi.acm.org/10.1145/224170.224228>.
- [17] Herman, A., 2015. Discrete-element bonded particle sea ice model design, version 1.3 – model description and implementation. *Geoscientific Model Development Discussions* 8, 5481–5533.
- [18] Hibler, W.D., 1979. A dynamic thermodynamic sea ice model. *J. Phys. Oceanogr* 9, 815–846.
- [19] Hintermüller, M., Stadler, G., 2006. An infeasible primal-dual algorithm for total variation-based inf-convolution-type image restoration. *SIAM Journal on Scientific Computing* 28, 1–23.
- [20] Hunke, E.C., Dukowicz, J.K., 1997. An elastic–viscous–plastic model for sea ice dynamics. *Journal of Physical Oceanography* 27, 1849 – 1867.
- [21] Hutter, N., Losch, M., 2020. Feature-based comparison of sea ice deformation in lead-permitting sea ice simulations. *The Cryosphere* 14, 93–113.
- [22] Ip, C.F., Hibler, W.D., Flato, G.M., 1991. On the effect of rheology on seasonal sea-ice simulations. *Annals of Glaciology* 15, 17–25.
- [23] Kimmritz, M., Danilov, S., Losch, M., 2015. On the convergence of the modified elastic-viscous-plastic method for solving the sea ice momentum equation. *J. Comp. Phys.* 296, 90–100.
- [24] Kimmritz, M., Losch, M., Danilov, S., 2017. A comparison of viscous-plastic sea ice solvers with and without replacement pressure. *Ocean Modelling* 115, 59–69.
- [25] Koldunov, N., Danilov, S., Sidorenko, D., Hutter, N., Losch, M., Goessling, H., Rakowsky, N., Scholz, P., Sein, D., Wang, Q., Jung, T., 2019. Fast EVP Solutions in a High-Resolution Sea Ice Model. *Journal of Advances in Modeling Earth Systems* 11, 1269–1284.
- [26] Kreyscher, M., Harder, M., Lemke, P., Flato, G.M., 2000. Results of the sea ice model intercomparison project: Evaluation of sea ice rheology schemes for use in climate simulations. *Journal of Geophysical Research: Oceans* 105, 11299–11320. doi:<https://doi.org/10.1029/1999JC000016>.
- [27] Kwok, R., Hunke, E., Maslowski, W., Menemenlis, D., Zhang, J., 2008. Variability of sea ice simulations assessed with RGPS kinematics. *Journal of Geophysical Research: Oceans* 113.
- [28] Lemieux, J.F., Knoll, D., Tremblay, B., Holland, D., Losch, M., 2012. A comparison of the Jacobian-free Newton-Krylov method and the EVP model for solving the sea ice momentum equation with a viscous-plastic formulation: a serial algorithm study. *J. Comp. Phys.* 231, 5926–5944.
- [29] Lemieux, J.F., Tremblay, B., 2009. Numerical convergence of viscous-plastic sea ice models. *Journal of Geophysical Research: Oceans* 114.

- [30] Lemieux, J.F., Tremblay, B., Sedláček, J., Tupper, P., Thomas, S., Huard, D., Auclair, J., 2010. Improving the numerical convergence of viscous-plastic sea ice models with the Jacobian-free Newton-Krylov method. *J. Comp. Phys.* 229, 2840–2852.
- [31] Liu, X., Thomas, M., Titi, E.S., 2022. Well-posedness of Hibler’s dynamical sea-ice model. *Journal of Nonlinear Science* 32, 1–31.
- [32] Losch, M., Fuchs, A., Lemieux, J.F., Vanselow, A., 2014. A parallel Jacobian-free Newton-Krylov solver for a coupled sea ice-ocean model. *J. Comp. Phys.* 257, 901–911.
- [33] Mehlmann, C., 2019. Efficient numerical methods to solve the viscous-plastic sea ice model at high spatial resolutions. Ph.D. thesis. Otto-von-Guericke-Universität Magdeburg, Fakultät für Mathematik. URL: <http://dx.doi.org/10.25673/14011>.
- [34] Mehlmann, C., Danilov, S., Losch, M., Lemieux, J.F., Hutter, N., Richter, T., Blain, P., Hunke, E.C., Korn, P., 2021. Simulating linear kinematic features in viscous-plastic sea ice models on quadrilateral and triangular grids with different variable staggering. *Journal of Advances in Modeling Earth Systems* 13, e2021MS002523.
- [35] Mehlmann, C., Richter, T., 2017a. A finite element multigrid-framework to solve the sea ice momentum equation. *J. Comp. Phys.* 348, 847–861.
- [36] Mehlmann, C., Richter, T., 2017b. A modified global Newton solver for viscous-plastic sea ice models. *Ocean Modeling* 116, 96–107.
- [37] Mitchell, L., Muller, E.H., 2016. High level implementation of geometric multigrid solvers for finite element problems: applications in atmospheric modelling. *Journal of Computational Physics* 327, 1–18. URL: <http://arxiv.org/abs/1605.00492>, doi:10.1016/j.jcp.2016.09.037, arXiv:1605.00492.
- [38] Rampal, P., Bouillon, S., Olason, E., Morlighem, M., 2016. neXtSIM: a new Lagrangian sea ice model. *The Cryosphere* 10, 1055–1073.
- [39] Rathgeber, F., Ham, D.A., Mitchell, L., Lange, M., Luporini, F., McRae, A.T.T., Bercea, G.T., Markall, G.R., Kelly, P.H.J., 2016. Firedrake: automating the finite element method by composing abstractions. *ACM Trans. Math. Softw.* 43, 24:1–24:27. URL: <http://arxiv.org/abs/1501.01809>, doi:10.1145/2998441, arXiv:1501.01809.
- [40] De los Reyes, J., Gonzalez Andrade, S., 2009. Path following methods for steady laminar Bingham flow in cylindrical pipes. *ESAIM Mathematical Modelling and Numerical Analysis* 43, 81–117. doi:10.1051/m2an/2008039.
- [41] Richter, T., Mehlmann, C., 2017. An accelerated Newton method for nonlinear materials in structure mechanics and fluid mechanics, in: Radu, F., K.Kumar, Berre, I., Nordbotten, J., Pop, I. (Eds.), *Numerical Mathematics and Advanced Applications*, Springer. pp. 345–353. Enumath 2017 Bergen.
- [42] Ringeyen, D., Tremblay, L.B., Losch, M., 2021. Non-normal flow rules affect fracture angles in sea ice viscous-plastic rheologies. *The Cryosphere* 15, 2873–2888.
- [43] Rudi, J., Shih, Y.h., Stadler, G., 2020. Advanced Newton methods for geodynamical models of Stokes flow with viscoplastic rheologies. *Geochemistry, Geophysics, Geosystems* 21.
- [44] Ruge, J.W., Stüben, K., 1987. 4. Algebraic Multigrid. pp. 73–130. URL: <https://epubs.siam.org/doi/abs/10.1137/1.9781611971057.ch4>.
- [45] Tsamados, M.L., Feltham, D.L., Wilchinsky, A.V., 2013. Impact of a new anisotropic rheology on simulations of Arctic sea ice. *Journal of Geophysical Research: Oceans* 118, 91–107.

- [46] Tuhkuri, J., Polojärvi, A., 2018. A review of discrete element simulation of ice–structure interaction. *Philosophical Transactions of the Royal Society A: Mathematical, Physical and Engineering Sciences* 376, 20170335.
- [47] West, B., O’Connor, D., Parno, M., Krackow, M., Polashenski, C., 2021. Improving discrete element simulations of sea ice break up: Applications to Nares Strait. *arXiv preprint arXiv:2105.05143* .
- [48] Wilchinsky, A.V., Feltham, D.L., 2011. Modeling coulombic failure of sea ice with leads. *Journal of Geophysical Research: Oceans* 116.
- [49] Wright, S., 1997. *Primal-Dual Interior Point Methods*. SIAM, Philadelphia.
- [50] Zhang, J., 2021. Sea ice properties in high-resolution sea ice models. *Journal of Geophysical Research: Oceans* 126, e2020JC016686.
- [51] Zhang, J., Hibler III, W.D., 1997. On an efficient numerical method for modeling sea ice dynamics. *Journal of Geophysical Research: Oceans* 102, 8691–8702.